# POTENTIOMETRIC SCANNING ELECTROCHEMICAL MICROSCOPY FOR THE LOCAL CHARACTERIZATION OF THE ELECTROCHEMICAL BEHAVIOUR OF MAGNESIUM-BASED MATERIALS

Javier Izquierdo[a], Lívia Nagy[b], István Bitter[c], Ricardo M. Souto[a,d], Géza Nagy[b]

[a] *Department of Physical Chemistry, University of La Laguna, E-38200 La Laguna, Tenerife, Canary Islands, Spain*

[b] *Department of General and Physical Chemistry, Faculty of Sciences, University of Pécs, 7624 Pécs, Ifjúság útja 6, Hungary*

[c] *Budapest University of Technology and Economics, Budafoki u. 8, 1111 Budapest, Hungary*

[d] *Instituto Universitario de Materiales y Nanotecnologías, University of La Laguna, E-38200 La Laguna, Tenerife, Canary Islands, Spain*

**Abstract**

The applicability of scanning electrochemical microscopy for the local detection and quantification of relevant species participating in the corrosion of magnesium-based materials is presented. The iron-magnesium galvanic pair exposed to aqueous NaCl solution was adopted as model system for this purpose. $Mg^{2+}$ ion concentration and pH profiles were investigated using ion selective electrodes, containing a liquid membrane and $Sb/Sb_2O_3$ as sensor elements, respectively. Oxygen consumption at the substrate related to the cathodic reaction was also monitored with the antimony-based electrode though operated amperometrically. Data show a major production of hydroxyl anions at the cathodic sites as result of the oxygen reduction half-reaction, whereas in the vicinity of the magnesium surface pH is greatly affected by the anodic dissolution process instead. The later produces the release of metal cations accompanied by hydrogen evolution.

**Keywords:** potentiometric SECM, magnesium, pH, ion selective micropipettes, antimony electrode.

## 1. Introduction

Electrochemical corrosion is one major cause of economic losses in the industrialized countries [1]. Despite their attractive mechanical properties, most metals and alloys spontaneously undergo corrosion if certain conditions occur, especially in aqueous environments. Particularly, due to its high strength-to-weight ratio, magnesium and its alloys are attractive materials for several purposes in the automotive, aerospace, electronics and energy-production industries [2-5]. And they are often found in unavoidable contact with other metals such as aluminum or steel [5]. However, these materials lack stability against corrosion and usually require additional protection. In fact, thanks to its tendency to degrade in aqueous environments, it has been considered as a potential biodegradable and biocompatible material for non permanent implants

[6-9]. Moreover, its position in the galvanic series has allowed magnesium to be evaluated for the protection of other metals by acting as sacrificial anode, either as a component of a protective coating, or via direct galvanic connection [10-14]. Besides, several Mg-containing alloys like those aluminum-based ones, tend to suffer from preferential dissolution of this component, usually the most active in the material [5,15,16].

Local microcells are originated in a metallic material subjected to corrosion, with the subsequent spatial distributions of anodes and cathodes on its surface when left at its open circuit potential (OCP). In this way, dissolution occurs as result of metal oxidation at the anodes, whereas this process is maintained by the reduction of some species from the environment at the cathodes, usually oxygen in neutral and moderately alkaline media, or protons in acidic solutions. Since these local cells are originally formed within the range of micrometers and nanometers, a comprehensive understanding of the mechanistic aspects of corrosion requires the synthesis of data in those scales. Unfortunately, conventional electrochemical techniques lack spatial resolution and provide little information on behavior at sites of corrosion initiation or at defects. The recent advent of a variety of local probe techniques is greatly contributing to overcome these limitations when applied to the investigation of corrosion processes *in situ*. Following this trend, researchers are exploring a wide variety of methods to characterize local electrochemical processes, which range from the design of microelectrochemical cells and setups, to the use of scanning probe techniques [17]. Among the later scanning electrochemical microscopy (SECM) has become one of the most powerful microscopical techniques for corrosion research due to the wide variety of operation modes which contribute to give a great versatility to the technique [18-20].

The corrosion of metals produces local changes in the concentrations of ionic and molecular species present in the adjacent liquid phase. Thus, the $M^{z+}$ ions produced at the anodic sites are transferred under diffusion control to the bulk, and the system can be studied by amperometric SECM [21]. This feature has been exploited to image the generation of specific metal cations in several studies that include visualization of metastable pits on austenitic steel in situ by SECM at the open-circuit potential [22], to the detection of metal dissolution either from inclusions in alloys [23-25] or from defects in polymer-coated metals [10,26,27]. On the other hand, in a neutral aqueous media, the reaction of dissolved oxygen from the electrolyte at the cathodic areas may be analyzed through monitoring of the subsequent depletion of oxygen content in the solution volume adjacent to the cathodic sites [28-32]. However, for the detection of concentration distributions in certain corroding samples, especially for metals with sufficiently negative redox potentials in aqueous environments, the use of Pt microelectrodes is limited by the onset of oxygen reduction and hydrogen evolution reactions [10,27,31]. Thus, for effective amperometric operation of the SECM, it becomes necessary to either purge out oxygen and to use modified electrodes to avoid early evolution of hydrogen gas [33,34]. Yet, more robust and selective procedures are to be developed for the analysis of these metal cations in order to gain a better understanding of the mechanisms involved in corrosion and passivation. As it is well known, corrosion processes are dramatically affected by pH too. Furthermore, both corrosion half-cell reactions may lead to local changes in pH of the surrounding

environment. On one hand, alkalinization always occurs in the cathodic sites due to either $H^+$ consumption or $OH^-$ release, depending on nature of sample and electrolyte, and it may facilitate the formation of passive films. On the other hand, some corrosion-produced metal ions may undergo hydrolysis at the anodic sites, and consequently reduce the local pH, a feature that usually accelerates the corrosive attack. Though the extent of pH variation associated with the hydrolysis of metal ions mainly depends on the equilibrium constant for their hydrolysis process [35], thus greatly varying from one metal to another, it may become a major feature affecting the onset of local corrosion microcells Therefore, the measurement of the local alterations of pH in the vicinity of a corroding system and their time evolution is a matter of major interest.

In contrast, though rather scarcely applied, these physicochemical parameters may be studied using ion-selective electrodes (ISEs) as tips. In this case, the SECM is operated in the potentiometric mode [36-38], which gives greater chemical selectivity. The applicability of $Zn^{2+}$ ion-selective microelectrodes (ISMEs) for the study of model corrosion systems with SECM [39,40] has been recently demonstrated, similarly to what has already been achieved with the Scanning Ion Electrode Technique (SIET) [41]. In studies applying SIET, a variety of ion-selective systems has been investigated [42-50], including $Mg^{2+}$ species released during corrosion of the buried metal from defects operated on coated magnesium alloys [42,45,48]. Yet investigations of magnesium substrates with SECM have only been carried out in amperometric mode [51,52] or using the platinum tip for measurements of the electrolyte resistance between the tip and the substrate [53]. In those studies, visualization of active regions in the surface was accomplished, however selective potentiometric detection of the local concentration of the corrosion produced $Mg^{2+}$ ions was not attempted.

Most often liquid type microelectrodes have been employed for studying pH distributions above corroding metal surfaces [42-50]. Nevertheless, for corrosion purposes using SECM, it would be preferable to use microelectrodes based on the characteristics of certain oxides of transition metals such as antimony [54-56] and iridum [57]. These solid state microelectrodes are much more robust than ion selective micropipettes. Furthermore they have the ability to behave as double function electrodes. This means that while in potentiometric mode they detect local pH, they can also function as amperometric SECM tip to detect electroactive species.

In this work, we report preliminary results on the characterization of a model corrosion system formed by an iron-magnesium galvanic couple which were obtained from SECM measurements using antimony and $Mg^{2+}$-ion selective electrodes as the tips. The concentration distributions of dissolved oxygen and $Mg^{2+}$ ions, as well as the pH distributions that result of the galvanic corrosion process, were measured and analyzed in terms of the corrosion processes occurring in the system.

## 2. Experimental section

### *2.1. Chemicals and solutions*

High purity antimony in powder presentation (Aldrich) was employed for the fabrication of the antimony electrode. Solutions were prepared from Millipore deionised water and analytical grade chemicals. The inner reference solution employed in the lumen of the $Mg^{2+}$-ion selective microelectrode (ISE) was 10 mM $MgCl_2$ + 0.25 M KCl. Different concentrations of the same magnesium salt, dissolved in 10 mM NaCl solution, were employed for calibration of the ISE.

The ionophore employed in the fabrication of the $Mg^{2+}$ ISE was bis-N,N-dychlohexyl-malonamide, which was synthesized following the method described in reference [58]. The composition of the ion selective cocktail was the following: 2.1 wt.% ionophore, 34.0 wt.% high molecular weight poly(vinyl-chloride), and 63.9 wt.% o-nitrophenyl-octyl-ether. 70 mol.% potassium tetrakis(p-chloro-phenyl) borate was subsequently added. All the components in the ionophore membrane were supplied by Sigma-Aldrich. Ion-selective microelectrodes were prepared using micropipettes pulled from borosilicate glass capillaries B200-116-10 (Sutter, Novato, CA, USA). The inner wall of the pipette tips were hydophobized exposing them to a solution of dimethyldichlorosilane in carbon tetrachloride.

### *2.2. Samples and probesinstruments*

The galvanic Fe-Mg couple employed for this study consisted on one sheet of each metal immobilized in *Epofix* resin (Struers, Ballerup, Denmark). Iron was cut from 1 mm thick sheet of 99.99% purity purchased from Goodfellow Materials Ltd. (Cambridge, UK), in order to obtain a 1 mm x 2 mm strip. For the magnesium surface, metal ribbon of 99% purity supplied by Panreac (Barcelona, Spain), with a cross section of 200 µm x 3 mm, was employed. Both metal strips were fixed vertically in the resin, facing up their rectangle cross sections as the active surfaces to be analyzed. The separation between the two metals was ca. 5 mm, which was assumed to be enough distance to avoid alterations in either of the active metal areas due to the reactions taking place on the other one for the duration of the tests performed in this study. The resulting mount with the embedded metals had a circular top surface of 3 cm diameter. The surface of the specimen was flat ground with abrasive SiC paper up to 4000 grit, rinsed with ethanol, dried in air, and finally wrapped around laterally by sellotape that reached over the mount surface for about 6 mm. Thus a small container of approximately 5 ml of electrolyte was created for the microelectrochemical measurements.

The antimony electrode employed in SECM for combined amperometric/potentiometric operation was fabricated following the procedure described elsewhere [55]. In brief, the fabrication was initiated by heating the antimony powder in a melting pot with a gas flame. When antimony melted, it was introduced in a thick glass Pyrex capillary using syringe suction. The resulting, antimony filled capillary was then pulled manually with standard glass blowers technique using metallic tweezers. This resulted in a small diameter glass fiber filled with antimony. A pipette with 500 µm tip diameter was prepared from borosilicate glass capillary and a section of the previously prepared antimony fiber was inserted in its lumen with the tip reaching out for about 15 mm, whereas ca. 20 mm long staying in the lumen. Mercury metal and a copper

wire were then inserted into the lumen of the thicker capillary to provide electrical contact resulting in the assembly shown in **Figure 1A**. Loctite® adhesive was used to seal both ends. The final microelectrode had an antimony disk of 175 µm with an *RG* value of 2.9. The electrochemical response of the antimony microelectrode for amperometric operation was tested in two electrolytes, namely aerated 10 mM NaCl, and deaerated 5 mM $[Ru(NH_3)_6]Cl_3$ + 0.1 M NaCl solutions. Potentiometric operation was directed to monitor the effect of pH on the potential of the electrode. Calibration was performed using 9 buffer solutions covering the range 4 ≤ pH ≤ 12. A linear relationship between the potential of the antimony tip and the solution pH was observed between 4 and 11, and the slope of the calibration plot amounted 42.3 mV/pH unit.

Potentiometric ion-selective operation was performed using a conventional micropipette type $Mg^{2+}$-ISE, that was prepared with liquid internal filling solution and a silver chloride coated silver wire of 250 µm diameter, as internal reference electrode. Schematic drawing of the micropipette electrode is shown in **Figure 1B**. It was fabricated according to well established procedures [59,60]. In brief, two micropipettes were first pulled from one glass capillary, and subsequently silanized by introducing inside a few microliters of 5 vol.% dimethyldichlorosilane solution in carbon tetrachloride. The hydrophobic layer was obtained by keeping the micropipettes at $80^0$C in an oven for about 30 min. The ionophore cocktail was then filled into the micropipette by applying vacuum from the back side with an attached syringe. Finally, the internal solution was backfilled with the assistance of a very thin capillary attached to a syringe, and the Ag/AgCl was placed and fixed with Loctite® adhesive. Due to the relatively big size of the metal samples employed in this study, micropipettes with about 180 µm tip diameter were prepared and used. As it is well known micropipette ISE's can be easily prepared with submicron diameter, however it was not justified to use so small tips in this work, because they present bigger resistance and high noise picking up character.

### *2.3. Instruments*

Measurements were performed in an SECM equipment built by Sensolytics (Bochum, Germany), controlled with a personal computer. The electrochemical interface employed in the amperometric operation was an Autolab bipotentiostat provided with a frequency response analyzer (Metrohm, Herisau, Switzerland). In this case, the electrochemical cell was completed with an Ag/AgCl/KCl (3M) electrode as reference, and a Pt wire as counter electrode. Alternating current (AC) mode was also performed using these instrument and cell configurations. AC voltage signals of 10 $mV_{pp}$ amplitude around the open circuit potential of the tip in the electrolyte were applied. A total of 26 frequency values in the 351 to 55493 Hz frequency range were used, and the values spaced logarithmically. The same SECM instrument was employed for the potentiometric measurements using ion selective electrodes, though in this case a home made voltage follower based on a $10^{12}$ Ω input impedance operational amplifier was interconnected between the cell and the potentiometric input of the system.

## 3. Results

### *3.1. $Mg^{2+}$ distribution over the magnesium surface*

In order to study the distribution of $Mg^{2+}$ concentration in the electrolyte from metal corrosion, SECM in potentiometric operation was employed with a $Mg^{2+}$-ISE as probe. The metal sample was placed at the bottom of the small electrochemical cell, and the Mg ISE tip was fastened onto the tip holder. Before the test electrolyte was introduced in the cell, the tip was placed over the centre of Mg metal surface using the *X*, *Y* motors of the instrument. A video camera was employed to assist the process. Next, the tip was carefully moved towards the metal surface by means of the *Z* motor until ca. 75 μm vertical tip-substrate distance was reached. At this stage, the test solution was added to the measuring cell, the reference electrode was introduced, and the two metals in the sample were electrically connected at the rear of the sample by means of a copper wire. The evolution of the e.m.f. of the cell was monitored with the elapse of time. After a few minutes, a steady voltage was attained. Then the tip was slowly removed from the metal surface, at a speed of 5 μm/s moved upward, while recording the electrode potential at the ISE. Once the chosen maximum tip-substrate distance was reached, the tip-substrate distance was kept constant for two minutes, and subsequently the tip was moved down at the same rate, 5 μm/s, to approach the Mg metal surface again. The electrode potential vs. tip-substrate distance curves could be converted into $pMg^{2+}$ – tip-substrate distance plots using the calibration curve of the electrode. Normalized tip-substrate distances were used by determining the ratio between the tip radius, *a*, and the vertical tip-substrate distance, *d*. The $pMg^{2+}$ – *d/a* curves measured during the initial withdraw (black curve) and the subsequent approach (red curve) steps are shown in **Figure 2**. Next, the electric connection between the Fe and Mg metals was removed, and a new retreat $pMg^{2+}$ – *d/a* curve was registered for the electrically-disconnected magnesium metal (cf. the blue curve in Figure 2).

As it was expected, the $Mg^{2+}$ ion concentration was higher when the tip was placed closer to the substrate. Nevertheless, the approaching (black) and the withdrawing (red) experimental curves for the galvanically-coupled metals are quite different. This difference can be attributed to unavoidable convection in the electrolyte produced by the motion of the tip. That is, as the tip is moved, it displaces some electrolyte from the $Mg^{2+}$-rich surroundings of the metal to the bulk solution, resulting in the measurement of bigger values for ion concentration during the retreat movement. And the opposite behavior is observed when recording the approach curve.

Higher $pMg^{2+}$ data were determined when the two metals were disconnected. This indicates that magnesium dissolves less vigorously in the environment when it is not acting as sacrificial anode for iron. From the plots given in Figure 2, it is also obvious that when magnesium was galvanically-coupled to iron, the curves were rougher than the one determined over the unconnected metal. The origin of this fact could be explained with the assistance of the video camera, because gas evolution occurred on the surface of magnesium when the two metals were electrically connected. That is, gas evolution was not exclusively restricted to the iron strip, but it was even more vigorous over magnesium. It is known from basic chemistry

that the gas evolving at the magnesium - water interface must be hydrogen resulting from the reaction between this metal and water. Interestingly the magnesium acts as an anode in the Mg – Fe couple, but hydrogen is reduced during its corrosion protecting function, a distinctive feature for this metal and its alloys [5].

The electric connection of the two metals originates the development of a high negative potential on the iron metal. It was observed to be more negative than -1.60 V vs. Ag/AgCl/KCl (3M) at all times. These potential values lay outside the stability range of water. And hydrogen gas evolution is also occurring at the iron surface.

Concentration profiles of $Mg^{2+}$ ions were also determined by rastering the ISE parallel to the surface. Line scans were measured along the 200 µm cross section of the Mg area, both with (red curve) and without (black curve) galvanic connection between the two metals. Results are given in **Figure 3** for single scan lines determined when the tip was maintained at ca. 75 µm vertical distance from the surface. As it was observed before, the signal registered near the corroding metal indicated higher $Mg^{2+}$ concentration when the metal was acting as sacrificial anode in the iron-magnesium galvanic pair, than those measured when the two metals were disconnected. The maximum dissolution of magnesium was detected when the tip passed over the central position of the metal strip, which supports that the whole area was behaving anodically. Conversely, this maximum over the center of the Mg stripe surface was not observed when the metals were not connected. In this case, the concentration profile was not symmetric in shape over the metal, and a separation between the portion acting as the anode (at the left side of the line scan), and the area functioning as hydrogen-reducing cathode (right side), could be noticed.

Additionally, several concentration profiles were measured at different locations over the Mg strip while the metal was under galvanic connection. In this way, heterogeneities in the location of the corrosion process over the metal could be detected. **Figure 4** depicts six concentration profiles measured when the tip was moved along the *X* axis at different *Y* positions, covering a total length of 100 µm in the *Y* axis, whereas keeping the same scan direction used to record Figure 3. That is, scanned *X* lines correspond to several of the cross sections taken in the 200 µm width direction of the magnesium area, which were measured over a central region of the larger 3 mm side. Despite the fact that the tip is actually too large to spatially resolve the system in these dimensions, the concentration profile measured for *Y* = 20 µm shows the higher values, indicating a region in the anodic surface of the metal displaying greater electrochemical activity. Further studies would be necessary to determine the actual heterogeneity of the whole system and the eventual generation of corrosion pits as result of it.

### *3.2. Oxygen consumption*

When a sacrifice anode is used for corrosion protection, oxygen consumption occurs at the cathodic sites of the protected metal surface if these metals are placed in non-acidic environments. In order to study

the oxygen concentration profile over the protected iron surface, an antimony microelectrode was employed as the SECM measuring tip while the technique operated in the amperometric mode. Since the SECM was operated in the amperometric mode, the tip-substrate distance could be adjusted using the negative feedback effect when approaching a zone of the resin sleeve located between the two metals. Furthermore, variations in the local oxygen concentration can also be visualized. For this purpose, the electrode was placed as close to the surface of the iron strip as possible with the assistance of a video camera, and subsequently retracted 1000 μm in the *Z* direction. Next, the tip was shifted horizontally 1.5 mm to be located above the resin sleeve. After the test electrolyte was added to the system, and while the two metals were kept electrically disconnected, the *Z*-approach curve was recorded. A constant potential of -0.70 V vs. Ag/AgCl/KCl (3M) was applied to the tip, a potential value at which oxygen reduction occurs. The closest tip-substrate distance in *Z*-approach curve shown in **Figure 5** occurs for a negative feedback of ca. 60% (black curve). This reduction in the faradic current measured at the tip corresponds to a height of 85 μm over the surface if we consider the electrode to be a microelectrode of 175 μm diameter with *RG* = 2.9 [61]. After this curve was recorded, the tip was lifted up, and moved parallel to the surface to a position located just above the center line of the iron strip to record the corresponding *Z*-approach curve. The same scan parameters were employed as before, still without galvanic connection between the two metals. The corresponding approach plot is also given in Figure 5 (blue curve). Though it could be expected that the corrosion of the disconnected iron should result in some oxygen consumption, the negative feedback effect actually seemed to be smaller on iron than above the resin. This apparent discrepancy could be explained by considering differential polishing on the resin and the metal piece. That is, due to the difference in hardness between the materials, the metal sample can be expected to protrude above the surrounding resin holder. Indeed, the Z-approach curve measured above the iron strip could be superimposed over that obtained on the resin by slightly shifting the curve along the *X* axis. In the forecoming, this observed distance difference was taken into account in order to establish the actual tip-substrate distance. On the other hand, the fact that the Z-approach curves measured both on the resin and on the iron strip could be superimposed, indicates that the extent of iron corrosion in this environment does not lead to a significant depletion of the oxygen concentration at early exposures.

On the other hand, the red curve in Figure 5 shows the Z-approach curve measured above the same location on iron strip that was measured after the two metals were electrically connected. In this case, local depletion of oxygen is readily observed in the plot. Thus, the corrosion of Mg drives a very intensive electrochemical oxygen reduction at the iron surface. And oxygen diffusion from the bulk electrolyte could not compensate its consumption at the metal.

Two dimensional images of oxygen consumption were obtained when the antimony tip made was scanned surface in an *X-Y* plane set at 175 μm vertical tip-substrate distance, and they are shown in **Figure 6**. Image A was recorded when the two metals were disconnected metals, while image B was achieved when they were galvanically-coupled. In Figure 6A, the image of iron substrate in Figure 6A shows up among the surrounding epoxy areas. Above the iron surface smaller current values were

registered, showing smaller oxygen concentrations could be obtained. We can conclude that the SECM image shows the corrosion of iron in this environment. On the other hand, the image of the iron strip shown in Figure 6B is much sharper. In this case, tip currents close to 0 nA were measured over the metal, thus showing that oxygen was absent from the thin electrolyte volume comprised between the tip and the iron strip. The dimensions of the area showing the lowest current values in the image closely match the dimensions of the iron surface (1 mm x 2 mm). This proves that the whole metal is behaving as a cathode. Therefore, the iron strip is effectively protected from corrosion through its connection with the sacrificial anode of magnesium.

### *3.3. pH distributions*

The antimony electrode was also employed to image pH distributions over the substrate during the corrosion reaction. Though the electrode was usually placed as close as possible to the investigated surface with the assistance of a video camera, the possibility to more precisely establish the tip-to-substrate distance by applying an alternating potential to the tip was investigated. In this way, the tip could remain unbiased, provided a sufficiently small excitation AC signal was employed. The rationale for not polarizing the antimony tip was to avoid the chemical modification of the $Sb/Sb_2O_3$ surface of the electrode. Alternating-current (AC) operation of the SECM was employed, and the magnitude of the current and its phase shift with respect to the applied AC potential modulation were recorded as impedance values. The near-field interaction between the SECM tip and the surface could be employed to obtain AC Z-approach curves within the frequency range. A location above the insulating resin, approximately equidistant from both metal specimens, was chosen for the determination of the tip-substrate distance, and the result is given in **Figure 7**. The plots depict the variation of the normalized modulus (Figure 7A), and the phase shift (Figure 7B) of the impedance as the tip approached the substrate for a selection of frequencies of the AC perturbation. Modulus values have been normalized by dividing the value recorded at each point by that measured in the bulk solution (e.g., sufficiently far from the substrate to give a stationary value). The higher impedance observed at the end of the curve for every frequency and the decrease in phase angle, are indications of the greater resistance offered to ionic current flow when the tip approached the insulating surface due to the smaller electrolyte volume, though the extent of this blocking effect greatly depends on the frequency of the AC excitation signal. Greater contrast was observed in the low-frequency range, whereas the system became very noisy at 55 kHz.

Once, when the very close tip-substrate distance was established with AC mode of SECM, the antimony tip was removed to a height of 80 μm, and subsequently positioned over the center of the magnesium sample, or the iron strip by moving the tip in the *X*-*Y* plane. Then, the potentiometric operation mode was set in order to monitor pH distributions over the metals. Vertical pH profiles were determined over the centre line of each of the metals, both when they were disconnected, and when galvanic contact was established between them. In these experiments the following protocol was followed: First, the pH-

sensitive ISE was removed from the surface to a distance of 600 µm. After 10 s waiting time at this height, the tip was moved down towards the surface until a tip-substrate distance of 0.5 normalized (*d/a*) units. After 10 s waiting time, the tip was removed again from the surface of the metal to the bulk. The potential of the ISE was continuously recorded during all the duration of the experiment. Tip movement in the vertical direction was always performed at the speed of 5 µm/s. In this way, vertical pH profiles could be obtained as a function of the normalized tip-substrate distance for both the approach and the retreat steps. The same protocol was employed while the two metals were electrically disconnected, and when they were galvanically coupled. **Figure 8** shows the mentioned vertical pH profiles measured above Mg surface. As it can be seen, in the case of the free-corroding magnesium sample, higher alkalinity is detected in the vicinity of the Mg surface (see Figure 8A), which indicates that the cathodic half-reaction takes place on some regions of the metal due to its free corrosion. The pH values determined at the largest distances were close to the corresponding value for the bulk solution, which was measured to be 8.76 when registered with a conventional pH-meter. Though the approach and retreat curves exhibit a similar behavior, they could not be overlapped, and they showed the biggest gap for normalized distances smaller than 1.5. This fact can be attributed to the forced convection effect produced by the tip during its movement to and from the surface. Higher pH values were measured during the retracting process in the major part of the displacement, because the electrode was departing from a portion of the electrolyte more concentrated in hydroxide anions during its movement from the surface towards the bulk of the solution.

The opposite trend was observed when galvanic connection was ensured (cf. Figure 8B). The pH of electrolyte adjacent to the magnesium surface became smaller, than the pH of the bulk. Close to the metal surface, pH values as low as 5.5 could be detected. This shift to the acidic direction occurred despite hydrogen evolution could still be observed with the video camera, and thus a source of alkalinization was still somehow active at the metal. However, the higher presence of protons is more difficult to evaluate due to the greater diffusion rate of this species and, in this specific case, also due to the noise in the system provoked by the evolution of hydrogen gas. The same effect was observed when the tip was moved parallel to the surface to record the scan line given in **Figure 9**. This latest measurement shows a clear pH decrease in a section of ca. 200 µm, which corresponds with the actual *X* portion of the magnesium strip used as target. It must be noticed that the onset of acidification could be detected at larger distances as a result of the diffusion of $H^+$ and $Mg^{2+}$ ions.

Finally, **Figure 10** displays pH – vertical *d/a* plots obtained above iron surface when the two metals were connected. In both plots, namely approach and retreat curves, the alkalinization observed near the cathode is extensive, even at distances as large as 2 mm. It is interesting to compare this result with the amperometric curve recorded for oxygen detection, previously shown in Figure 6B, when the limiting current was attained at *d/a* values of ca. 5. That is, constant oxygen concentration in the electrolyte close to the bulk solution value could already be found at a tip-substrate distance of 900 µm. Certainly, the corrosion process originates an increase in the solution pH here through the reduction of oxygen. But in combination with the amperometric observations, if that was the only source of this effect, $OH^-$

concentration should decrease down to the values in bulk solution at much smaller tip-substrate distances than those found in Figure 10. Then, hydrogen evolution, probably resulting from the highly negative OCP experienced by the electrically connected system, is likely to be the additional factor that leads to this high pH in the proximity of the iron strip. It must be noted that pH values shown in Figure 10 for the volume of electrolyte in the vicinity of the iron surface are far beyond the dynamic measuring range of the antimony electrode. Therefore no quantitative information can be extracted from these curves.

## 4. Discussion

We report here that potentiometric operation of the SECM can be employed to locally measure concentration distributions of key species involved in the corrosion of magnesium in aqueous solution. This metal is very reactive in water, thus making difficult to design accurate experiments to study its corrosion mechanism. At present, despite the rather extensive literature on the corrosion of this metal and its alloys, the origin of the corrosion process is still obscure and subjected a big controversy, and a number of experimental observations are regarded by some researcher as dubious. Even experimental techniques are often put to their limits when investigating the electrochemical behaviour of magnesium in aqueous solutions due to joint operation of several features, namely:

(1) The high dissolution rate of the metal in contact with an aqueous environment often leads to portions of the material being physically detached from the matrix. It also makes difficult the safe removal of corrosion products from the uncorroded material. As a result, weight-loss measurements may bear big experimental errors. Furthermore, they are average measurements that give no information on the dynamics of the corrosion reactions.

(2) The corrosion of the magnesium is accompanied by vigorous hydrogen evolution [3,4]. A “strange hydrogen evolution behaviour” has been described [5]. That is, more hydrogen is evolved when the anodic overvoltage is increased or a higher anodic current density is imposed, conversely to what happens with the other metals. This phenomenon is called the negative difference effect (NDE). Hydrogen evolution can greatly affect the efficiency of electrochemical probes either by blocking their surface or even modifying their surface state. Additionally, it causes convection effects in the electrolyte solution that affect the current distribution in the electrochemical cell. Conversely, experimental methods have been developed for the quantification of hydrogen evolving during the corrosion of magnesium and its alloys [62]. Though they may be regarded highly efficient techniques, and procedures have been designed to follow the variation with time of hydrogen evolution, they cannot distinguish whether the gas evolves from anodic or cathodic sites.

(3) Magnesium hydrolysis is basically non-acidic. The equilibrium constant associated with the first deprotonation step of its aquo-complexes $[M(H_2O)_x]^{2+}$, has $pK_a^1$ = 11.4 [63]. The acidification

caused by hydrolysis of $Mg^{2+}$ can be calculated for given concentrations of the metal ion using the equation:

$$pH = -\log\sqrt{K_a^1 \cdot [Mg^{2+}]} \quad (1)$$

Using $[Mg^{2+}]$ = 0.0001 and 0.1 M, the expected pH values would be 7.0 and 6.2, respectively [41]. That is, oxidation of magnesium is not capable of significantly changing the pH of a neutral corrosion medium. Conversely, either oxygen or proton electroreduction during the cathodic half-cell reaction produce strong alkaline environments. Strong alkaline environments are usually reported around corroding magnesium and magnesium alloys [5].

(4) The formation of a passive film of magnesium hydroxide that exhibits some corrosion protection characteristics is considered to be formed on magnesium and its alloys, especially at high pH [64]. This passive film is unstable, and the onset of corrosion on magnesium is regarded to occur at film-free areas on the surface of the metal [5,53,65]. Indeed, the open circuit potential of fresh polished samples immersed in aqueous environments usually evolves towards more noble potentials [5,53], until a “pitting potential” is attained at which breakdown of the surface film occurs [3,66,67]. Though pitting potential and pit nucleation are terms frequently employed in the literature related to the corrosion of this metal, stable pit growth has not been described for magnesium and magnesium alloys [35]. Conversely, retrieved samples show that the entire exposed surface has been corroded [35].

Scanning electrochemical microscopy was selected as the experimental technique for this work as to gain new spatially-resolved information concerning the chemical reactions responsible for the corrosion of CP magnesium. A special concern was taken in relation to identify if alkalinization occurred at both the anodic and cathodic microcells formed on the metal, or whether diffusion of the high concentration of hydroxyl ions formed in the cathodes were responsible for the alkalinization of the electrolyte. Though a small electrolyte volume is typically employed in SECM experiments, the choice of a small magnesium strip insulated in a much bigger resin mount was considered to allow enough dilution of the formed $OH^-$ species as to detect the source of these ions at least for the early stages of metal corrosion. Additionally, the mount contained also an iron strip, thus allowing some experiments to be conducted with galvanic coupling of the two metals, which can be simply attained by electrically connecting the two strips at the back of the mount. In this way, separation of the anodic and cathodic sites could be achieved if the two metal strips were separated enough in the mount, though at the cost of an increase of the corrosion rate of magnesium. Figures 2 and 3 show significantly smaller pMg values in a thin electrolyte layer above the magnesium strip following the galvanic coupling of this metal to iron. That is, the use of a $Mg^{2+}$ ion-selective microelectrode (ISME) allowed for concentration distributions of the dissolved metal to be measured. It must also be noticed that despite the enhancement of magnesium dissolution due to the galvanic-coupling to iron, the dimensions of the magnesium strip were sufficient for the amount of dissolved magnesium never to

saturate the detection limit of the ISME (see supplementary material). That is, the microelectrode probe was sensitive to changes in the concentrations of $Mg^{2+}$ for the duration of the experiments, contrary to the expectations made by other Authors [5]. Another important outcome from our work is obtained from inspection of Figure 4. Though the magnesium strip was working as the anode in the Fe-Mg galvanic pair, dissolution of the metal does not occur simultaneously over the entire exposed surface. Indeed, it has been observed from a sequence of SECM measurements passing over the same scan lines (not shown), that the locations of high $Mg^{2+}$ concentrations are shifted over the exposed magnesium strip. Our experiments, still of some preliminary nature, agree thus well with the previous observations made using SVET by Williams and McMurray [35]. We are currently working on the fabrication of more robust ion-selective electrodes with smaller internal resistances, that will allow higher scan rates to be used with SECM, thus allowing maps rather than selected scan lines to be recorded.

Another important outcome of this work was the observation of oxygen consumption when magnesium was galvanically connected to iron. This dissolved species in the solution was consumed in the thin electrolyte volume located over the iron strip when acting as the cathode during the corrosion of magnesium. Indeed, the amperometric SECM images in Figure 6 clearly demonstrate that the enhanced corrosion rate of magnesium when galvanically-coupled to iron directly corresponds to an enhancement in the consumption of oxygen, despite the occurrence of hydrogen evolution on the metal. Simultaneously, the pH in the thin electrolyte volume located above the magnesium strip becomes slightly acidic, attaining values between 5.5 and 6. These values are only slightly more acidic than those predicted by application of equation (1) considering the hydrolysis of $Mg^{2+}$ ions in the electrolyte. Values as low as 5.3 have already been reported from SIET measurements on corroding AZ31 magnesium alloy, which was ascribed to the co-dissolution and hydrolysis of Al along with Mg, since this alloy contains ca. 3% aluminium. In the case of CP magnesium, the possible contribution of minute amounts of iron, even in small amounts in the order of ppm [68], may justify the more acidic values found in our work. Since the $pK_a^1$ of Fe is more than two units smaller than that of Al (2.2 and 4.5, respectively) [63], a 0.0001 M $Fe^{2+}$ solution of produces almost the same pH decrease than another 0.1 M in $Al^{3+}$ [41]. Not only the pH values can be justified on the basis of the physicochemical response of CP magnesium, but they are well inside the linear response of the antimony microelectrode with pH [56]. Again the design of the experiment has satisfactorily served for pH monitoring of magnesium corrosion in an aqueous solution, without meeting the warnings raised in ref. [5]. This feature is very important when considering that no alkalinization was observed around the anodic sites in any of the experiments described in our work. And alkalinization is a requirement for the occurrence of the chemical reaction suggested to account for the negative difference effect (NDE) [65,69]. In this model, formation of $Mg^+$ species and their direct reaction with water, is proposed:

$$2\,H^+ + 2\,e^- \rightarrow H_2\uparrow \qquad \text{(cathodic partial reaction)} \qquad (2)$$

$$2\,Mg \rightarrow 2\,Mg^+ + e^- \qquad \text{(anodic partial reaction)} \qquad (3)$$

$$2\,Mg^{+} + 2\,H_2O \rightarrow 2\,Mg^{2+} + 2\,OH^{-} + H_2\uparrow \text{ (chemical reaction)} \qquad (4)$$

From equation (4), both the consumption of protons and the production of $OH^-$ are expected at the anodic sites on corroding magnesium. Another implication is that hydrogen gas evolution should occur at those sites. Yet, evolution of hydrogen gas from the corroding magnesium sample can be explained by taking in account the previous observations by Williams and McMurray [35]. In their work on the corrosion of magnesium in concentrated chloride solution investigated by SVET, they observed that the anodic sites occupy only a (small) fraction of the area exposed to the electrolyte, and that local cathodes can develop in very near proximity to them on the previously corroded surface. Therefore, hydrogen evolution do not necessarily must occur at the actual anodic microcell sites, but could occur on the surrounding cathodic area. The results reported in this work could be well described using the same interpretation. This explanation may hold even in the case of magnesium galvanically-coupled to iron. Though the major part of the cathodic reaction occurs on the separated iron strip, some cathodic areas might still develop on the magnesium sample in the close proximity to the corroding anodic sites. The development of such minute cathodic sites in the otherwise anodic metal in a galvanic couple has been recently observed in our laboratory using a combination of scanning microelectrochemical techniques for the Fe-Zn galvanic system [70]. This interpretation also accounts for the electrolyte resistance SECM images given in ref. [53], in which the anodic activity on a free corroding magnesium sample occurred only on a small fraction of the exposed surface.

## 5. Conclusion

The applicability of the $Mg^{2+}$-ISE to characterize magnesium-based materials by SECM has been demonstrated. The results show that anodic dissolution of magnesium anodes takes place preferentially in certain most active sites. The increase in $Mg^{2+}$ ion concentration occurring in the vicinity of the magnesium strip, was found to be two orders of magnitude bigger when the nature of the degradation process changed from spontaneous self-corrosion to galvanic corrosion. Imaging of oxygen concentration distribution and pH detection were carried out with the antimony electrode, and it was possible to clearly distinguish anodic and cathodic behaviors occurring simultaneously on the same surface. Thus, the combination of measurements and electrodes presented here allowed to identify and to quantify the different reactions taking place during the corrosion process. Additionally, the results open a promising new route to the elucidation of certain characteristics of the mechanism involved in the corrosion and passivation of magnesium, which result from greatly localized reactions.

## Acknowledgements

The authors are grateful to the Spanish Ministry of Science and Innovation (MICINN, Madrid, Acción Integrada No. HH2008-0011) and to the National Office for Research and Technology (NKTH, Budapest, research grant ES-25/2008 TeT) for the grant of a Collaborative Research Programme between Hungary and Spain. J.I. and R.M.S. are grateful for financial support by the MICINN and the European Regional Development Fund (Brussels, Belgium) under Project No. CTQ2009-12459. A Research Training Grant awarded to J.I. by the MICINN (Programa de Formación de Personal Investigador) is gratefully acknowledged. L.N. and G.N. acknowledge support from "Developing Competitiveness of Universities in the South Transdanubian Region (SROP-4.2.1.B-10/2/KONV-2010-0002)". The Authors acknowledge valuable discussions with Dr. Nick Birbilis during the preparation of the manuscript.

**References:**

[1] M.V. Biezma, J.R. San Cristóbal, *Corros. Eng. Sci. Technol.* 40 (2005) 344-352.

[2] G.L. Makar, J. Kruger, *Int. Mater. Rev.* 38 (1993) 138-153.

[3] G. Song, A, Atrens, *Adv. Eng. Mater.* 1 (1999) 11-33.

[4] G. Song, A. Atrens, *Adv. Eng. Mater.* 5 (2003) 837-858.

[5] G. Song, *Adv. Eng. Mater.* 7 (2005) 563-586.

[6] F. Witte, *Acta Biomater.* 6 (2010) 1680-1692.

[7] N.T. Kirkland, J. Lespagnol, N. Birbilis, M.P. Staiger, *Corros. Sci.* 52 (2010) 287-291.

[8] S. Virtanen, *Mater. Sci. Eng. B* 176 (2011) 1600-1608.

[9] N.T. Kirkland, N. Birbilis, M.P. Staiger, *Acta Biomater.* 8 (2012) 925-936.

[10] A.M. Simões, D. Battocchi, D.E. Tallman, G.P. Bierwagen, *Corros. Sci.* 49 (2007) 3838-3849.

[11] A.M. Simões, D. Battocchi, D.E. Tallman, G.P. Bierwagen, *Prog. Org. Coat.* 63 (2008) 260-266.

[12] P.C.R. Varma, B. Duffy, J. Cassidy, *Surf. Coat. Technol.* 204 (2009) 277-284.

[13] D. Wang, G.P. Bierwagen, *Prog. Org. Coat.* 64 (2009) 327-338.

[14] P. Volovitch, T.N. Vu, C. Allély, A.A. Aal, K. Ogle, *Corros. Sci.* 53 (2011) 2437-2445.

[15] J. Wloka, G. Bürklin, S. Virtanen, *Electrochim. Acta* 53 (2007) 2055-2059.

[16] F.M. Queiroz, M. Magnani, I. Costa, H.G. de Melo, *Corros. Sci.* 50 (2008) 2646-2657.

[17] P. Marcus, F. Mansfeld (Eds.): *Analytical Methods in Corrosion Science and Engineering*. CRC Press, Boca Raton, FL, 2006.

[18] L. Niu, Y. Yin, W. Guo, M. Lu, R. Qin, S. Chen, *J. Mater. Sci.* 44 (2009) 4511-4521.

[19] S.E. Pust, W. Maier, G. Wittstock, *Z. Phys. Chem.* 222 (2008) 1463-1517.

[20] R.M. Souto, S.V. Lamaka, S. González, in: *Microscopy: Science, Technology, Applications and Education*, vol. 3; A. Méndez-Vilas, J. Díaz, (Eds.). Formatex Research Center, Badajoz (Spain), 2010, pp. 1769-1780.

[21] J.V. Macpherson, P.R. Unwin, in: *Scanning Electrochemical Microscopy*; A.J. Bard, M.V. Mirkin (Eds.). Marcel Dekker, New York, 2001, pp. 521-592.

[22] Y. González-García, G.T. Burstein, S. González, R.M. Souto, *Electrochem. Commun.* 6 (2004) 637-642.
[23] C.H. Paik, H.S. White, R.C. Alkire, *J. Electrochem. Soc.* 147 (2000) 4120-4124.
[24] C.H. Paik, R.C. Alkire, *J. Electrochem. Soc.* 148 (2001) B276-B281.
[25] K. Fushimi, M. Seo, *Electrochim. Acta* 47 (2001) 121-127.
[26] R.M. Souto, Y. González-García, S. González, *Corros. Sci.* 47 (2005) 3312-3323.
[27] S. González, J.J. Santana, Y. González-García, L. Fernández-Mérida, R.M. Souto, *Corros. Sci.* 53 (2011) 1910-1915.
[28] A.C. Bastos, A.M. Simões, S. González, Y. González-García, R.M. Souto, *Electrochem. Commun.* 6 (2004) 1212-1215.
[29] A.M. Simões, A.C. Bastos, M.G. Ferreira, Y. González-García, S. González, R.M. Souto, *Corros. Sci.* 49 (2007) 726-739.
[30] R.M. Souto, L. Fernández-Mérida, S. González, *Electroanalysis* 21 (2009) 2640-2646.
[31] J.J. Santana, J. González-Guzmán, L. Fernández-Mérida, S. González, R.M. Souto, *Electrochim. Acta* 55 (2010) 4488-4494.
[32] Y. González-García, J.M.C. Mol, T. Muselle, I. de Graeve, G. van Assche, G. Scheltjens, B. van Mele, H. Terryn, *Electrochem. Commun.* 13 (2011) 169-173.
[33] R.M. Souto, Y. González-García, D. Battistel, S. Daniele, *Chem. Eur. J.* 18 (2012) 230-236.
[34] R.M. Souto, Y. González-García, D. Battistel, S. Daniele, *Corros. Sci.* 55 (2012) 401-406.
[35] G. Williams, H.N. McMurray, *J. Electrochem. Soc.* 155 (2008) C340-C349.
[36] G. Denuault, G. Nagy, K. Tóth, in: *Scanning Electrochemical Microscopy*; A.J. Bard, M.V. Mirkin (Eds.). Marcel Dekker, New York, 2001, pp. 397-444.
[37] G. Nagy, L. Nagy, *Fresenius J. Anal. Chem.* 366 (2000) 735-744.
[38] G. Nagy, L. Nagy, *Anal. Lett.* 40 (2007) 3-38.
[39] Á. Varga, L. Nagy, J. Izquierdo, I. Bitter, R.M. Souto, G. Nagy, *Anal. Lett.* 44 (2011) 2876-2886.
[40] J. Izquierdo, L. Nagy, Á. Varga, I. Bitter, G. Nagy, R.M. Souto, *Electrochim. Acta* 59 (2012) 398-403.
[41] S.V. Lamaka, R.M. Souto, M.G.S. Ferreira, in: *Microscopy: Science, Technology, Applications and Education*, vol. 3; A. Méndez-Vilas, J. Díaz (Eds.). Formatex Research Center, Badajoz (Spain), 2010, pp. 2162-2173.
[42] S.V. Lamaka, O.V. Karavai, A.C. Bastos, M.L. Zheludkevich, M.G.S. Ferreira, *Electrochem. Commun.* 10 (2008) 259-262.
[43] M.F. Montemor, W. Trabelsi, S.V. Lamaka, K.A. Yasakau, M.L. Zheludkevich, A.C. Bastos, M.G.S. Ferreira, *Electrochim. Acta* 53 (2008) 5913-5922.
[44] S.V. Lamaka, G. Knörnschild, D.V. Snihirova, M.G. Taryba, M.L. Zheludkevich, M.G.S. Ferreira, *Electrochim. Acta* 55 (2009) 131-141.
[45] S.V. Lamaka, M.G. Taryba, M.L. Zheludkevich, M.G.S. Ferreira, *Electroanalysis* 21 (2009) 2447-2453.

[46] A.C. Bastos, M.G. Taryba, O.V. Karavai, M.L. Zheludkevich, S.V. Lamaka, M.G.S. Ferreira, *Electrochem. Commun.* 12 (2010) 394-397.

[47] D. Snihirova, S.V. Lamaka, M. Taryba, A.N. Salak, S. Kallip, M.L. Zheludkevich, M.G.S. Ferreira, M.F. Montemor, *ACS Appl. Mater. Interf.* 2 (2010) 3011-3022.

[48] O.V. Karavai, A.C. Bastos, M.L. Zheludkevich, M.G. Taryba, S.V. Lamaka, M.G.S. Ferreira, *Electrochim. Acta* 55 (2010) 5401-5406.

[49] S.V. Lamaka, M. Taryba, M.F. Montemor, H.S. Isaacs, M.G.S. Ferreira, *Electrochem. Commun.* 13 (2011) 20-23.

[50] M. Taryba, S.V. Lamaka, D. Snihirova, M.G.S Ferreira, M.F. Montemor, W.K. Wijting, S. Toews, G. Grundmeier, *Electrochim. Acta* 56 (2011) 4475-4488.

[51] X. Liu, T. Zhang, Y. Shao, G. Meng, F. Wang, *Corros. Sci.* 51 (2009) 1772-1779.

[52] M.D. Pereda, C. Alonso, M. Gamero, J.A. del Valle, M.F.L. de Mele, *Mater. Sci. Eng. C* 31 (2011) 858-865.

[53] G. Baril, G. Galicia, C. Deslouis, N. Pébère, B. Tribollet, V. Vivier, *J. Electrochem. Soc.* 154 (2007) C108-C113.

[54] B. Horrocks, M.V. Mirkin, D.T. Pierce, A.J. Bard, G. Nagy, K. Toth, *Anal. Chem.* 65 (1993) 1213-1224.

[55] J. Izquierdo, L. Nagy, Á. Varga, J.J. Santana, G. Nagy, R.M. Souto, *Electrochim. Acta* 56 (2011) 8846-8850.

[56] J. Izquierdo, L. Nagy, J.J. Santana, G. Nagy, R.M. Souto, *Electrochim. Acta* 58 (2011) 707-716.

[57] D.O. Wipf, F. Ge, T.W. Spaine, J.E. Baur, *Anal. Chem.* 72 (2000) 4921-4927.

[58] K. Tóth, E. Lindner, M. Horváth, J. Jeney, E. Pungor, I. Bitter, B. Ágai, L. Töke, *Electroanalysis* 5 (1993) 781-790.

[59] R.C. Thomas, Ion-selective intracellular microelectrodes: How to make and use them. Academic Press, London, 1978.

[60] D. Ammann. Ion-selective microelectrodes. Principles, design and application. Springer-Verlag, Berlin, 1986.

[61] M.V. Mirkin, in: A.J. Bard, M.V. Mirkin (Eds.), Scanning Electrochemical Microscopy. Marcel Dekker, New York, 2001, pp. 145-199.

[62] G.L. Song, A. Atrens, D. StJohn, *Magnesium Technology 2001*, TMS, New Orleans, 2001, pp. 255-262.

[63] Y.Y. Lur'e, *Handbook of Analytical Chemistry* (In Russian, Spravochnik po analiticheskoi himii), 6th edition. Himiya, 1989.

[64] A.-M. Lafront, W. Zhang, S. Jin, R. Tremblay, D. Dubé, E. Ghali, *Electrochim. Acta* 51 (2005) 489-501.

[65] G. Song, A. Atrens, *Adv. Eng. Mater.* 9 (2007) 177-183.

[66] G. Song, A. Atrens, X. Wu, B. Zhang, *Corros. Sci.* 40 (1998) 1769-1791.

[67] G. Song, A. Atrens, M. Dargush, *Corros. Sci.* 41 (1999) 249-273.

[68] Z. Qiao, Z. Shi, N. Hort, N.I.Z. Abidin, A. Atrens, *Corros. Sci.* 61 (2012) 185–207.

[69] A. Atrens, W. Dietzel, *Adv. Eng. Mater.* 9 (2007) 292-297.

[70] J. Izquierdo, S. González, L. Fernández-Mérida, R.M. Souto, under preparation.

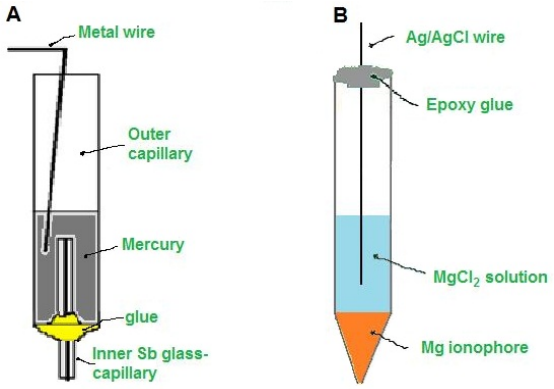


**Figure 1**
Sketches of the two types of potentiometric tips employed in the SECM measurements: (A) antimony electrode, and (B) micropipette-based $Mg^{2+}$-ISE (containing $10^{-2}$ M $MgCl_2$ + 0.25 M KCl as the internal solution).

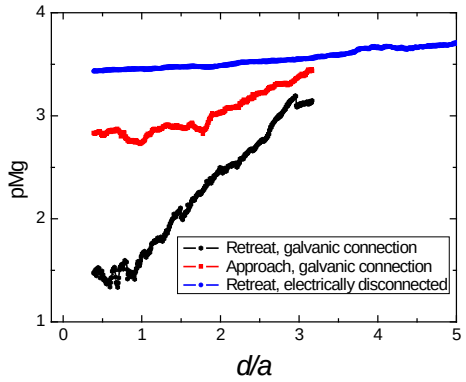


**Figure 2**
Distribution of $Mg^{2+}$ ion concentration above the magnesium strip measured with the $Mg^{2+}$-ISE as the height of the tip is changed. The iron-magnesium sample was immersed in 10 mM NaCl solution, whereas the two metals were either connected electrically (i.e. galvanic coupling) or disconnected. Both the direction of the tip movement and the electrical condition of the metal are given in the graph. *d/a* is the dimensionless distance between the sample and the tip. Scan rate: 5 μm $s^{-1}$.

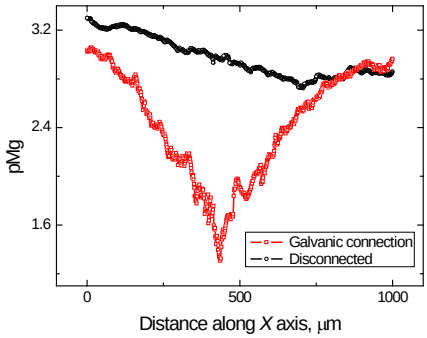


**Figure 3**
Potentiometric SECM scan lines measured above the magnesium strip in the iron-magnesium sample during immersion in 10 mM NaCl. The metals were: (– □ –) with, and (– ○ –) without galvanic connection. Vertical tip-substrate distance: 75 μm; scan rate: 5 μm/s.

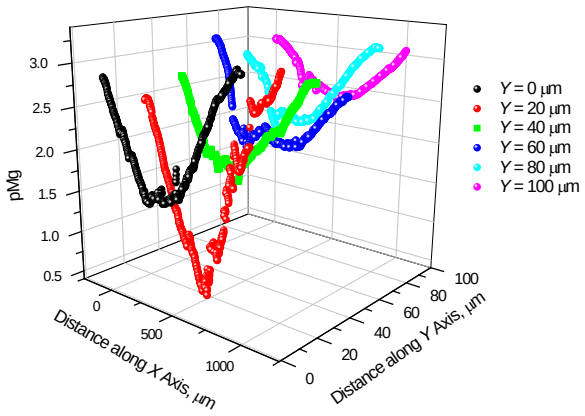


**Figure 4**
Potentiometric SECM scan lines measured when the tip crossed crossing (*X* direction) over the magnesium strip in the iron-magnesium galvanic pair immersed in 10 mM NaCl, taken in a plane parallel to the surface of the metal. The different curves were obtained after shifting the tip in the *Y* direction in 20 µm steps. Tip-substrate distance: 75 µm; scan rate: 5 µm/s.

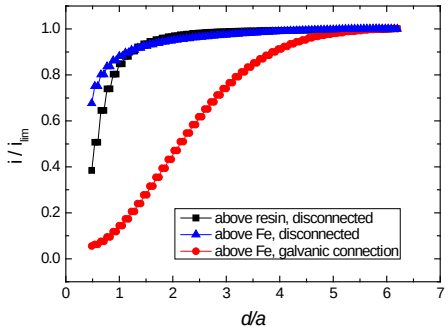


**Figure 5**
Normalized *Z*-approach curves measured with the antimony electrode in amperometric SECM operation using oxygen reduction at the tip as redox mediator reaction. The plots were measured above the resin sleeve or the iron strip as indicated in the graph. were performed when The iron and the magnesium strips were either disconnected, or connected electrically during the experiments, as indicated in the legend. Test electrolyte: 10 mM NaCl. Tip potential: -0.70 V vs. Ag/AgCl/KCl (3M); scan rate: 10 µm/s; tip diameter: 175 µm; *RG* = 2.9. $i/i_{lim}$ is the dimensionless tip current, and *d/a* is the dimensionless distance between the sample and the tip.

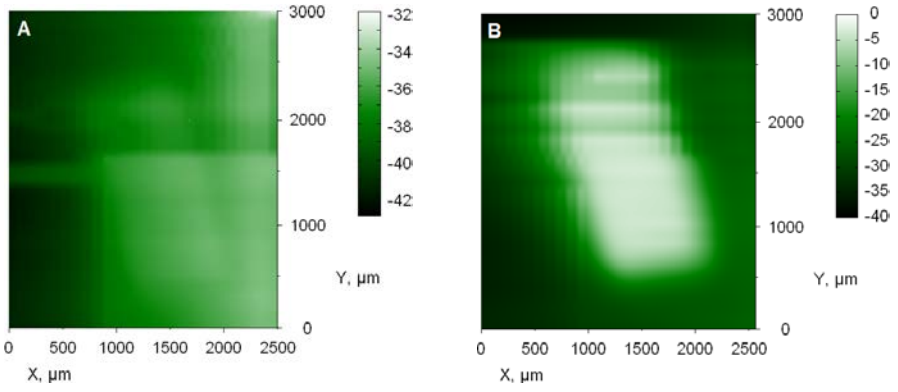


**Figure 6**
Amperometric SECM images depicting the absolute current measured at the antimony tip travelling over the iron strip when the iron-magnesium sample was immersed in 10 mM NaCl. The metals were: (A) without, and (B) with galvanic connection. Tip potential: -0.70 V vs. Ag/AgCl/KCl (3M); tip diameter: 175 µm; *RG* = 2.9; tip-substrate distance: 175 µm; scan rate: 30 µm/s. The figures represent an area of 2500 µm x 3000 µm in *X* and *Y* directions.

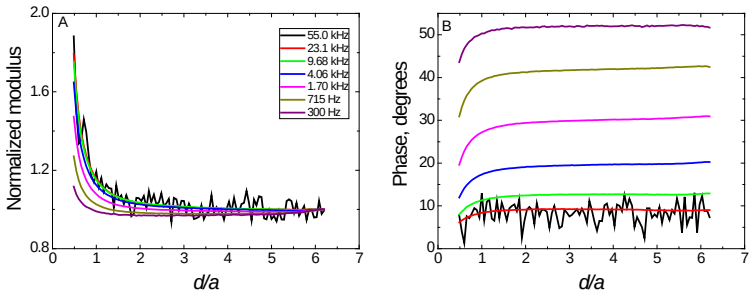


**Figure 7**
Normalized AC *Z*-approach curves towards the resin sleeve at a position located between the iron and the magnesium strips when the sample was immersed in 10 mM NaCl with the 175 µm antimony electrode. The tip was left at its spontaneous open-circuit potential in the electrolyte (namely +0.44 V vs. Ag/AgCl/KCl (3 M)). The excitation signal amplitude was 10 $mV_{pp}$, and frequencies are indicated in the figure. (A) Normalized magnitude, and (B) phase of the impedance measured at the tip. *d/a* is the dimensionless distance between the sample and the tip.

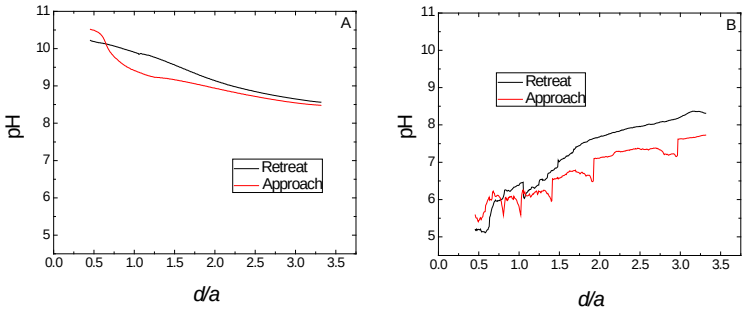


**Figure 8**
pH distributions above the magnesium strip measured with the antimony tip as its height was changed relative to the surface. The iron-magnesium sample was immersed in 10 mM NaCl, whereas the two metals were (A) disconnected, and (B) galvanically-coupled. The direction of the tip movement is indicated in the figures; scan rate: 5 µm/s. *d/a* is the dimensionless distance between the sample and the tip.

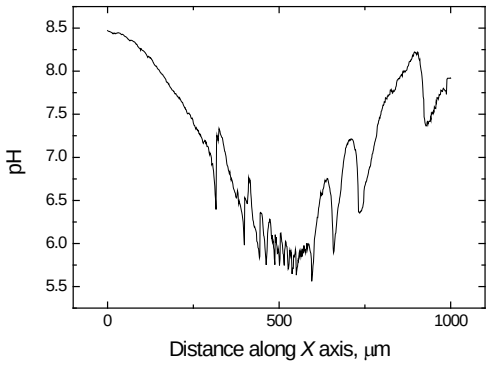


**Figure 9**
pH distribution during a scan line recorded with the antimony electrode over the magnesium strip. The iron-magnesium galvanic pair was immersed in 10 mM NaCl. Tip-substrate distance: 80 µm; scan rate: 5 µm/s.

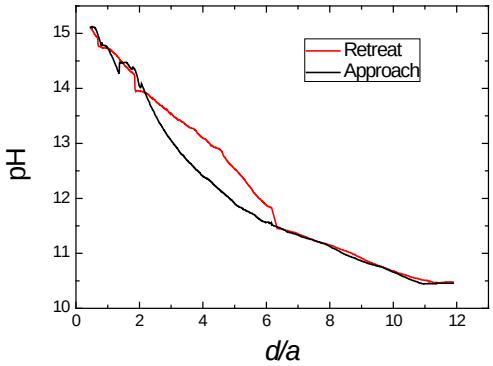


**Figure 10**
pH distributions above the iron strip measured with the antimony tip as its height was changed relative to the metal surface. The iron-magnesium galvanic pair was immersed in 10 mM NaCl. The direction of the tip movement is indicated in the figures; scan rate: 5 µm/s.